# Experimental Confirmation of the Optoelectronic Reciprocity Theorem in High-Efficiency $CuIn_{1-x}Ga_xSe_2$ Solar Cells

Hajime Shibata,[1,*] Jiro Nishinaga,[1] Yukiko Kamikawa,[1] Hitoshi Tampo,[2] Takehiko Nagai,[2] Takashi Koida,[2] Shogo Ishizuka,[1] Toshimitsu Mochizuki,[3] and Masafumi Yamaguchi[4]

[1] *Global Zero Emission Research Center, National Institute of Advanced Industrial Science and Technology (AIST), 1-1-1 Umezono, Tsukuba, Ibaraki 305-8568 Japan*

[2] *Research Institute for Energy Conservation, National Institute of Advanced Industrial Science and Technology (AIST), 1-1-1 Umezono, Tsukuba, Ibaraki 305-8568 Japan*

[3] *Renewable Energy Research Center, National Institute of Advanced Industrial Science and Technology (AIST), 2-2-9 Machiikedai, Koriyama, Fukushima 963-0298, Japan*

[4] *Toyota Technological Institute, 1-12-1 Hisakata, Tempaku-ku, Nagoya 468-8511, Japan*

(Received 18 October 2022; revised 20 March 2023; accepted 3 April 2023; published 23 May 2023)

The optoelectronic reciprocity theorem has been proposed as a theorem relating electroluminescence (EL) and photovoltaic external quantum efficiency in solar cells. The theorem is vital for a fundamental understanding of solar cell operation and its application to device evaluation. Furthermore, with this theorem, it is also possible to estimate the open-circuit voltage ($V_{OC}$) of solar cells using the external radiative efficiency ($\eta_{ext}$) obtained from the absolute value of EL emission intensity, even for solar cells for which we cannot directly measure $V_{OC}$, such as subcells of multijunction solar cells or individual Si cells in modules and arrays. However, it is not *a priori* obvious that the optoelectronic reciprocity theorem holds for the various solar cells that exist. In this study, we report the results of qualitative and quantitative confirmation of the validity of the optoelectronic reciprocity theorem for high-efficiency $CuIn_{1-x}Ga_xSe_2$ (CIGS) solar cells fabricated by us. The results confirm that our CIGS solar cells qualitatively and quantitatively satisfy the optoelectronic reciprocity theorem within the limits of measurement uncertainty. Also, we experimentally confirm that the value of the diode ideality factor for the applied voltage dependence of the EL emission intensity is exactly unity when the emission mechanism is the band-edge emission due to the direct recombination of electron-hole pairs. Finally, the importance of the $\eta_{ext}$ for improving solar cell efficiency is explained.

DOI: 10.1103/PhysRevApplied.19.054072

## I. INTRODUCTION

Recently, there has been a dramatic increase in the demand for solar energy technology for green energy [1]. The development of high-performance solar cells could provide a reliable way to meet this demand. To develop highly efficient solar cells, it is vital to know how much room is left for improvement in the open-circuit voltage ($V_{OC}$). Therefore, it is essential to understand the theoretical limits of $V_{OC}$ for solar cells under development.

Shockley and Queisser calculated the theoretical limit of solar cell performance using the principle of detailed balance. This principle states that "the rate of photon emission due to recombination is equal to the rate of absorption of the same photon, when solar cells are in thermal equilibrium" [2]. Both rates were given by $F_{c0}$ in Eq. (3.1) in the original paper by Shockley and Queisser, which is the essential point of the Shockley and Queisser theories. The reason is that the theoretical limit value of the reverse saturation current in the *p-n* junction $I_{0,SQ}$ is given by $I_{0,SQ} = qF_{c0}$, where $q$ is the elementary charge.

In addition, the very important concept of external radiative efficiency ($\eta_{ext}$), which is an effective index of the room for improvement left in $V_{OC}$, has been introduced [3–27]. The following equation expresses the relationship between $\eta_{ext}$ and $V_{OC}$ when the emission mechanism is the band-edge emission due to the direct recombination of electron-hole pairs:

$$V_{OC} = V_{OC,em} + \left(\frac{k_B T}{q}\right) \ln \eta_{ext}, \tag{1}$$

where $k_B$ is the Boltzmann constant, and $V_{OC,em}$ is the theoretical limit of $V_{OC}$ because it is the $V_{OC}$ at $\eta_{ext} = 100\%$, which means no nonradiative recombination. Therefore, if the values of $V_{OC,em}$ are known, the value of $V_{OC}$ can be estimated by substituting the measured value of $\eta_{ext}$ into

*h.shibata@aist.go.jp

 

Eq. (1), even for solar cells for which we cannot directly measure the value of $V_{OC}$, such as subcells of multijunction solar cells [15] or individual Si cells in modules and arrays [16].

One way to know the values of $V_{OC,em}$ is to use the optoelectronic reciprocity theorem. The optoelectronic reciprocity theorem for solar cells gives a reciprocal relationship between the light absorption and light emission properties of devices, and has been studied as follows. First, van Roosbroeck and Shockley [28] described the relationship between the photoluminescence (PL) emission spectrum and the optical absorption coefficient spectrum. Lasher and Stern [29] extended the relationship to nonthermal equilibrium states by considering the effects of quasi-Fermi-level splitting (QFLS). Würfel [30] extended the relationship to the electroluminescence (EL) emission of light-emitting diodes (LEDs) and verified the relationship between QFLS and applied voltage $V$. The first application of the theory was made by Green *et al.*, who applied it to LEDs to develop high-efficiency silicon LEDs [31]. Subsequently, the theory was applied to solar cells by Rau and Werner [32] and Werner *et al.* [33], and finally organized by Rau [3] to give the following equation for; $qV \gg k_BT$:

$$\phi_{em}(E) = \mathrm{EQE}(E)\phi_{BB}(E)\exp\left(\frac{qV}{k_BT}\right), \tag{2}$$

where $\phi_{em}(E)$ denotes the EL emission spectrum when voltage $V$ is applied, where $E$ is the photon energy. EQE($E$) is the photovoltaic external quantum efficiency when the direction of the incident light is perpendicular to the solar cell surface. In addition, the following equation expresses $\phi_{BB}(E)$ which is a black body emission spectrum at absolute temperature $T$, where $h$ and $c$ are the Planck constant and the speed of light in vacuum, respectively.

$$\phi_{BB}(E)=\left(\frac{2\pi}{h^3c^2}\right)\left(\frac{E^2}{e^{E/k_BT}-1}\right).$$

Therefore, if we let $V_{OC,em}$ be $V_{OC,rad}$ when the optoelectronic reciprocity theorem holds, we have

$$V_{OC,rad} = \left(\frac{k_BT}{q}\right)\ln\left(\frac{J_{SC}}{J_{0,rad}}\right), \tag{3}$$

where $J_{SC}$ is the short-circuit current density, and $J_{0,rad}$ is given by the following:

$$J_{0,rad} = q\int_0^\infty \mathrm{EQE}(E)\phi_{BB}(E)dE. \tag{4}$$

This $V_{OC,rad}$ is called the radiative limit of $V_{OC}$. Then, substituting $V_{OC,em}$ in Eq. (1) with $V_{OC,rad}$, we obtain the following equation:

$$V_{OC} = V_{OC,rad} + \left(\frac{k_BT}{q}\right)\ln\eta_{ext}. \tag{5}$$

Therefore, we can estimate the value of $V_{OC}$ using Eq. (5) when the optoelectronic reciprocity theorem holds, even in solar cells for which we cannot directly measure the value of $V_{OC}$, by measuring $\eta_{ext}$, EQE($E$) and calculating $V_{OC,rad}$ using Eqs. (3) and (4).

However, it is not *a priori* obvious that the optoelectronic reciprocity theorem of Eq. (2) holds in the various solar cells that exist; there are cases where Eq. (2) does not hold even qualitatively, as reported in Müller *et al.* [13]. Mattheis *et al.* [34] successfully reproduced the PL emission spectrum from the absorptance spectrum by considering fluctuations in the energy position of the fundamental absorption edge in the absorptance spectrum of $CuIn_{1-x}Ga_xSe_2$ (CIGS) solar cells. For $c$-Si and CIGS solar cells, Kirchartz and Rau [4] first confirmed that Eq. (2) qualitatively holds, i.e., the following equation holds,

$$\phi_{em}(E) \propto \mathrm{EQE}(E)\phi_{BB}(E). \tag{6}$$

They did not consider fluctuations in the fundamental absorption edge for their analysis, because the gradient of the Ga : In composition ratios of their samples was different from those of Mattheis *et al.* [34]. Furthermore, they examined whether Eq. (2) was quantitatively valid. That is, they confirmed whether Eq. (5) holds for $c$-Si and CIGS solar cells, although they used the current density that was about 3 times the $J_{SC}$ when they measured the values of $\eta_{ext}$. Delamarre *et al.* [9] confirmed that Eq. (2) holds for GaAs solar cells both qualitatively and quantitatively by taking the effect of series resistance into account. Mochizuki *et al.* [16] confirmed both qualitatively and quantitatively that Eq. (2) holds for Si solar cells.

Theoretically, some reports have predicted that the optoelectronic reciprocity theorem does not hold in some cases. Kirchartz *et al.* [6] showed by simulation that the optoelectronic reciprocity theorem does not hold in *p-i-n* junction solar cells whose carrier mobility is extremely low or whose main carrier recombination mechanism is the Shockley-Read-Hall mechanism. Also, Aeberhard and Rau [18] and Toprasertpong *et al.* [25] showed by simulation that the optoelectronic reciprocity theorem does not hold when the thickness of the space-charge region is greater than that of the quasineutral region.

In this paper, we report the results of qualitative and quantitative confirmation of the validity of the optoelectronic reciprocity theorem given by Eq. (2) for high-efficiency CIGS solar cells fabricated by us.

## II. EXPERIMENT AND METHODS

Let $J_{\rm dark}(V)$ be the dark $J$-$V$ characteristic. Let $J_{\rm em}(V)$ be the number of electrons converted to photons based on the radiative recombination per unit time. By using $\phi_{\rm em}(E)$ introduced in Sec. I, $J_{\rm em}(V)$ is given as

$$J_{\rm em}(V) = q\int_0^\infty \phi_{\rm em}(E)dE. \tag{7}$$

Therefore, if we let $J_{\rm em}(V)$ be $J_{\rm rad}(V)$ when the optoelectronic reciprocity theorem holds and substitute Eq. (2) into Eq. (7), we have

$$J_{\rm rad}(V) = J_{0,\rm rad}\exp\left(\frac{qV}{k_BT}\right), \tag{8}$$

where $J_{0,\rm rad}$ is given by Eq. (4). $J_{\rm em}(V)$ is most generally given by

$$J_{\rm em}(V) = J_{0,\rm em}\exp\left(\frac{qV}{nk_BT}\right), \tag{9}$$

where $J_{0,\rm em}$ denotes the prefactor when the optoelectronic reciprocity theorem does not hold, and $n$ denotes the diode ideality factor. Theoretically, the value of $n$ is exactly unity when the EL emission mechanism is band-edge emission due to the direct recombination of electron-hole pairs. However, we generalize the formula and leave it as $n$. Therefore, if the voltage $V_{\rm OC,em}$ is defined as the voltage satisfying $J_{\rm em}(V_{\rm OC,em}) = J_{\rm SC}$, it is given by

$$V_{\rm OC,em} = \left(\frac{nk_BT}{q}\right)\ln\left(\frac{J_{\rm SC}}{J_{0,\rm em}}\right). \tag{10}$$

If the optoelectronic reciprocity theorem holds and the EL emission mechanism is the band-edge emission due to the direct recombination of electron-hole pairs, Eq. (10) reproduces Eq. (3).

As noted in Sec. I, we report the results of qualitative and quantitative confirmation of the validity of the optoelectronic reciprocity theorem given by Eq. (2) for high-efficiency CIGS solar cells fabricated by us. The methods used are as follows. First, we qualitatively validate that Eq. (2) holds, implying that Eq. (6) holds. However, in this study, we use the PL emission spectrum $\phi_{\rm PL}(E)$ instead of $\phi_{\rm em}(E)$ to achieve this. In other words, we experimentally measure $\phi_{\rm PL}(E)$ and EQE$(E)$ and confirm that

$$\phi_{\rm PL}(E) \propto {\rm EQE}(E)\phi_{\rm BB}(E). \tag{11}$$

Then, we quantitatively confirm that Eq. (2) holds. The methods are summarized as steps (i)–(iv):

(i) Measure the EQE$(E)$ spectrum and calculate the value of $J_{0,\rm rad}$ using Eq. (4).

(ii) Experimentally determine $J_{\rm em}(V)$ by measuring the absolute value of the EL emission intensity.

(iii) Fit Eq. (9) to the observed $J_{\rm em}(V)$ to determine the most probable values of $J_{0,\rm em}$ and $n$.

(iv) Compare the value of $J_{0,\rm rad}$ with $J_{0,\rm em}$ to examine whether they are equal.

Therefore, the uncertainties of $J_{0,\rm rad}$ and $J_{0,\rm em}$ are very important subjects in this study. We define the relative standard uncertainties of $J_{0,\rm rad}$ and $J_{0,\rm em}$ as $u_{\rm rad}$ and $u_{\rm em}$, respectively. In fact, $u_{\rm em}$ is larger than $u_{\rm rad}$, as discussed in the following. Therefore, in this study, we quantitatively confirm the validity of the optoelectronic reciprocity theorem by examining whether the value of $J_{0,\rm rad}$ falls within the range of $J_{0,\rm em}(1\pm u_{\rm em})$. We also examine whether the results of the fitting in step (iii) yield $n = 1$.

However, it is vital to note that if we cannot neglect the influence of the series resistance, the value of the net voltage applied to the $p$-$n$ junction $V_{\rm int}$ is different from the nominal applied voltage $V$ as follows:

$$V_{\rm int} = V - R_{\rm ser}J, \tag{12}$$

where $R_{\rm ser}$ is the series resistance of the cell and $J$ is the density of the current flowing through the cell. Therefore, in this study, we consider $V_{\rm int}$ instead of $V$ in Eqs. (1)–(9).

The CIGS absorber layer with a thickness of about 2 μm is fabricated by a three-step process using elemental Cu, In, Ga, and Se Knudsen cell sources in a vacuum chamber on a soda-lime glass substrate with a Mo back contact deposited on it by dc sputtering. Therefore, the variation in the thickness direction of the band gap of the CIGS thin film used in this study has a double grading structure [35]. The substrate temperatures for stages I, II, and III are 350, 550, and 550 °C, respectively. Then a CdS buffer layer with a thickness of about 30 nm is fabricated on the CIGS absorption layer using the chemical bath deposition method. A ZnO layer is deposited on the CdS layer by rf sputtering and an $n$-type ZnO : Al layer is deposited on it by dc sputtering. The thicknesses of the intrinsic ZnO and $n-$ZnO : Al layers are about 0.06 and 0.35 μm, respectively. Then, an Al grid electrode is formed on the $n$-ZnO : Al layer by electron-beam evaporation. Finally, an antireflection film of $MgF_2$ is deposited with a thickness of 110 nm by thermal evaporation.

The device studied here comprises eight cells fabricated on a single substrate. In this study, we measure the $J$-$V$ characteristics, PL spectra, EQE$(E)$ spectra, and the absolute value of EL emission intensity to obtain $J_{\rm em}(V_{\rm int})$. We use the measurement system called the WSL-2000 SCREMS developed by the ATTO Corporation to measure the absolute value of EL emission intensity [36]. Here, it is vital to note that we can measure only the number of photons with WSL-2000 SCREMS; the EL emission spectrum

is unmeasurable. The methods for measuring $J_{\rm em}(V_{\rm int})$ by WSL-2000 SCREMS are summarized as steps (i)–(iii):

(i) Take an EL image with an appropriate exposure time $T_0$ for a given $V_{\rm int}$.
(ii) Analyze the obtained EL image and obtain $n(V_{\rm int})$, the number of photons that pass through the camera's lens during the exposure time $T_0$.
(iii) Convert $n(V_{\rm int})$ to $J_{\rm em}(V_{\rm int})$.

The actual procedure is as follows. First, let $\Omega_0$ be the solid angle from the surface of the device looking into the camera lens, which is $\Omega_0 = 2.95 \times 10^{-3}$ sr in this study. Next, an EL image is taken with an exposure time of $T_0$ for a given $V_{\rm int}$. Then, if $\Omega_0 \ll 1$, $n(V_{\rm int})$ is given by

$$n(V_{\rm int}) = \left(\frac{T_0 A_c \Omega_0}{\pi}\right) \int_0^\infty \phi_{\rm em}(E) dE. \tag{13}$$

Here, the factor $\pi$ appears because we assume that the angular dependence of EL emission intensity follows Lambert's cosine law. $A_c$ is the area of the front surface of the solar cell, which is $A_c = 0.522$ cm$^2$. Then $J_{\rm em}(V_{\rm int})$ is expressed using $n(V_{\rm int})$,

$$J_{\rm em}(V_{\rm int}) = q\left(\frac{\pi}{T_0 A_c \Omega_0}\right) n(V_{\rm int}). \tag{14}$$

By substituting Eq. (13) into Eq. (14), we have Eq. (7). Experimentally, $n(V_{\rm int})$ is obtained as follows. The signal intensity $L(V_{\rm int})$ measured using ATTO WSL-2000 SCREMS is defined as

$$L(V_{\rm int}) = T_0 A_c \left(\frac{\Omega_0}{\pi}\right) \int_0^\infty \phi_{\rm em}(E) S(E) dE,$$

where $S(E)$ denotes the sensitivity of the measurement system. Then $n(V_{\rm int})$ is obtained as

$$n(V_{\rm int}) = \frac{L(V_{\rm int})}{S_{\rm eff}}, \tag{15}$$

where $S_{\rm eff}$ denotes the effective sensitivity of the system and is determined to satisfy the following equation:

$$S_{\rm eff} \int_0^\infty \phi_{\rm em}(E) dE = \int_0^\infty \phi_{\rm em}(E) S(E) dE. \tag{16}$$

Roughly speaking, $S_{\rm eff}$ is the average value of $S(E)$ in the region where $\phi_{\rm em}(E) > 0$. Therefore, the value of $S_{\rm eff}$ will be close to $S(E_0)$ if $\phi_{\rm em}(E)$ has a sharp peak at $E = E_0$. However, in practice in this study, we use $\phi_{\rm PL}(E)$ rather than $\phi_{\rm em}(E)$ to determine the value of $S_{\rm eff}$. Therefore, $S_{\rm eff}$ is practically determined to satisfy the following equation,

$$S_{\rm eff} \int_0^\infty \phi_{\rm PL}(E) dE = \int_0^\infty \phi_{\rm PL}(E) S(E) dE. \tag{17}$$

Here, we need only the relative value of $\phi_{\rm PL}(E)$ to determine $S_{\rm eff}$ using Eq. (17). Therefore, in this study, the absolute values of PL emission intensity are not calibrated, and only the relative values of $\phi_{\rm PL}(E)$ are measured.

In this study, the calibration of the absolute value of $S(E)$ is carried out as steps (1)–(3):

(1) Determine the relative value of the curve of $S(E)$, which is called the sensitivity curve.
(2) Calibrate the absolute value of $S(E)$ at $E = 1.08$ eV using the standard light source developed especially for this purpose.
(3) The absolute value of $S(E)$ is calibrated for all photon energies $E$.

Therefore, in summary, the following operations (i)–(v) are performed to determine the values of $J_{0,\rm em}$:

(i) Measure $\phi_{\rm PL}(E)$ and determine the value of $S_{\rm eff}$ using Eq. (17).
(ii) Measure the value of $L(V_{\rm int})$ using WSL-2000 SCREMS.
(iii) Calculate the value of $n(V_{\rm int})$ using Eq. (15).
(iv) Substitute the result into Eq. (14) to obtain $J_{\rm em}(V_{\rm int})$.
(v) Fit Eq. (9) to the obtained result to determine the most probable values of $J_{0,\rm em}$ and $n$.

In this study, we estimate the $\eta_{\rm ext}$ value. The quantum efficiency of the solar cell as an LED, i.e., $Q_{\rm LED}(V)$, is defined as

$$Q_{\rm LED}(V) \equiv \frac{J_{\rm em}(V)}{J_{\rm dark}(V)}. \tag{18}$$

Thus, we define the $\eta_{\rm ext}$ as

$$\eta_{\rm ext} \equiv Q_{\rm LED}(V_{\rm OC}). \tag{19}$$

By substituting Eq. (18) into Eq. (19) and assuming that $J_{\rm dark}(V_{\rm OC}) = J_{\rm SC}$, i.e., the "shifting approximation" [37] holds, we obtain the following:

$$\eta_{\rm ext} = \frac{J_{\rm em}(V_{\rm OC})}{J_{\rm SC}}. \tag{20}$$

The value of the $\eta_{\rm ext}$ is obtained using Eq. (20).

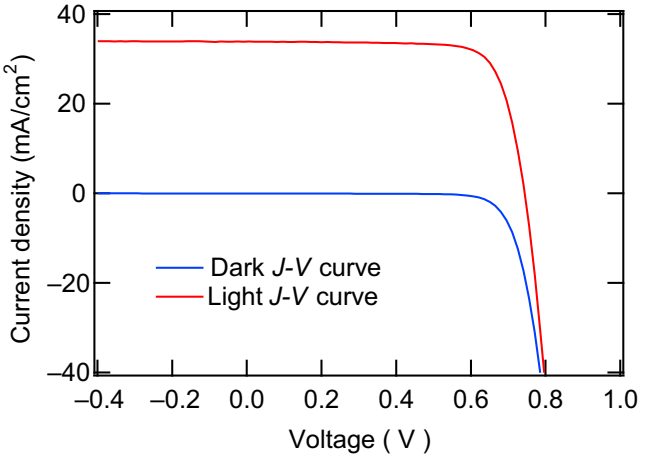


FIG. 1. Dark $J$-$V$ characteristics (blue curve) and light $J$-$V$ characteristics (red curve) of the CIGS solar cells used in this study.

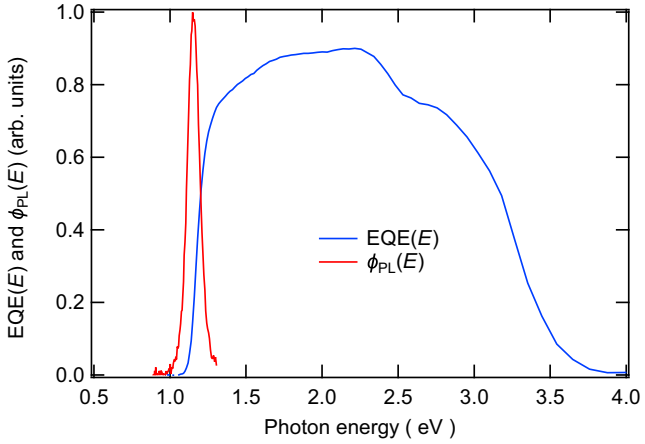


FIG. 2. EQE($E$) spectrum (blue curve) and PL emission spectrum $\phi_{PL}(E)$ (red curve) of the CIGS solar cells used in this study.

## III. RESULTS AND DISCUSSION

The eight cells used in this study are named SQ3720-3-1 to 8. Figure 1 shows the dark and light $J$-$V$ characteristics of the devices. Since the $J$-$V$ characteristics of the eight cells are analogous to each other, the results in Fig. 1 are their average values. Table I presents a summary of the solar cell parameters obtained from Fig. 1. Also, Table I shows the $R_{ser}$, $R_{sh}$, $J_0$, and $n$ values obtained by analyzing the dark $J$-$V$ characteristics, where $R_{sh}$ and $J_0$ denote the shunt resistance and saturation current density, respectively. Figure 2 shows the EQE($E$) spectrum of the devices used in this study as a blue curve. Because the EQE($E$) of the eight cells are analogous to each other, the results in Fig. 2 are their average value. The value of $J_{SC}$ calculated from the EQE spectrum is 32.66 mA/cm$^2$, which is very close to the value listed in Table I, with a relative difference of about 3.6%. Therefore, the uncertainty of the EQE spectrum shown in Fig. 2 is considered to be of the same order of magnitude. In Fig. 2, the red curve is the PL emission spectrum $\phi_{PL}(E)$. As stated before, this study measures only the relative values of $\phi_{PL}(E)$. The EQE($E$) shows that the band-gap energy $E_g$ is $E_g \approx 1.15$ eV. $\phi_{PL}(E)$ indicates that the PL emission spectrum is highly monochromatic and has a sharp peak at $E \approx E_g$. Therefore, the mechanism of the PL emission is considered to be band-edge emission. Hence, the mechanism of the EL emission of the eight cells is also deemed to be band-edge emission with a sharp peak at $E \approx E_g$. The blue circles in Fig. 3 represent the result of the calculated right-hand side of Eq. (11), and the red line is the PL spectrum. In Fig. 3, they are in good agreement, confirming that Eq. (11) is valid. Therefore, it can be qualitatively confirmed that the optoelectronic reciprocity theorem given by Eq. (2) holds for the CIGS solar cells studied in this work. The cause of some noise in the blue circles at $E < 1.1$ eV is that the value of EQE($E$) is small in that region.

Next, to accurately calculate the integral of the right-hand side of Eq. (4), we need to precisely extend the EQE($E$) spectrum in Fig. 2 to the lower-energy side. The reason is that the EQE($E$) on the right-hand side of Eq. (4) makes a significant contribution to the integration in the low-energy region, because $\phi_{BB}(E)$ has a high value in the region. According to Eq. (11), the result of dividing $\phi_{PL}(E)$ by $\phi_{BB}(E)$ at $T = 300$ K should have the same $E$ dependence as EQE($E$). In Fig. 4, the red curve is the result of dividing $\phi_{PL}(E)$ by $\phi_{BB}(E)$ at $T = 300$ K, and the blue circles are EQE($E$) in Fig. 2. Here, we multiply the red curve by an appropriate coefficient. The agreement between them is good, indicating that it is reasonable to use this method to extend EQE($E$) to the low-energy side [14]. Multiplying $\phi_{BB}(E)$ at $T = 300$ K to the EQE($E$) thus extended to the low-energy side, we obtain the integrand EQE($E$)$\phi_{BB}(E)$ of the right-hand side of Eq. (4) shown in the inset of Fig. 4 as a green curve. The result is in excellent agreement with the PL spectrum shown in Fig. 3, which is quite reasonable.

Then the function shown in the inset of Fig. 4 as a green curve is substituted into the right-hand side of Eq. (4) and

TABLE I. The solar cell parameters obtained from the dark and light $J$-$V$ characteristics in Fig. 1, where $\eta$ and FF are conversion efficiency and fill factor, respectively. The values of $R_{ser}$, $R_{sh}$, $J_0$, and $n$ are obtained by analyzing the dark $J$-$V$ characteristics.

| $\eta$ (%) | $V_{OC}$ (V) | $J_{SC}$ (mA/cm$^2$) | FF | $R_{sh}$ ($\Omega$cm$^2$) | $R_{ser}$ ($\Omega$cm$^2$) | $J_0$ (mA/cm$^2$) | $n$ |
|---|---|---|---|---|---|---|---|
| 19.5 | 0.74 | 33.9 | 0.77 | $1.2 \times 10^4$ | 0.69 | $1.50 \times 10^{-8}$ | 1.35 |

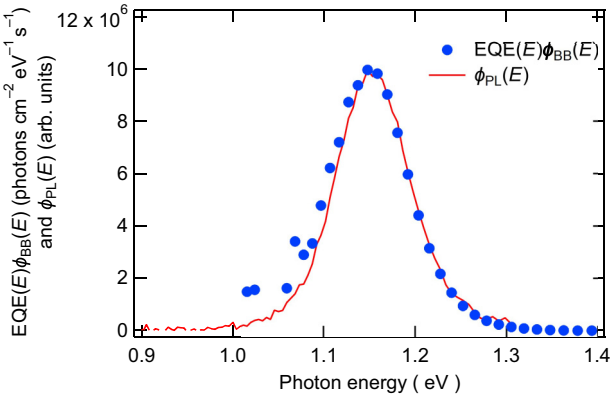


FIG. 3. Blue circles are the results of the right-hand side of Eq. (16) calculated using both EQE($E$) spectrum shown in Fig. 2 and $\phi_{\rm BB}(E)$ at $T = 300$ K. Red curve is the PL emission spectrum shown in Fig. 2.

by integrating, we obtain

$$\int_0^\infty {\rm EQE}(E)\phi_{\rm BB}(E)dE = 1.1 \times 10^6 \text{ photons m}^{-2}\text{ s}^{-1}. \tag{21}$$

Therefore, the value of $J_{0,\rm rad}$ given by Eq. (4) is expressed as

$$J_{0,\rm rad} = 1.8 \times 10^{-14}\ \text{mA/cm}^2. \tag{22}$$

Substituting the result of Eq. (22) into Eq. (3) to calculate the value of $V_{\rm OC,rad}$ yields the following result:

$$V_{\rm OC,rad} = 0.91\ \text{V}. \tag{23}$$

This result is illustrated diagrammatically in Fig. 5, along with the green curve showing $J_{\rm rad}(V_{\rm int})$ given by Eq. (8). Thus, the result of $E_g \approx 1.15$ eV yields $\Delta V_{\rm OC,rad} \equiv E_g/q - V_{\rm OC,rad} = 0.24$ V, which is very close to the value assumed in our previous study (0.23 V) [20–23] and reported by Yao *et al.* (0.231 V) [14]. As the relative uncertainty in the EQE spectrum is about 3.6%, as mentioned previously, the maximum relative uncertainty of the results of Eqs. (21)–(23) is considered to be about 5%, which implies that the maximum value of $u_{\rm rad}$ is also considered to be about 5%.

Table II shows the values of $J_{\rm em}(V_{\rm int})$ for the cells SQ3720-3-1 to 8 (units are mA/cm$^2$). Table II also shows the density of injected current $J_{\rm dark}$ and the value of the applied voltage $V$ when we measure the EL emission intensity, and value of $V_{\rm int}$ obtained from Eq. (12). Figure 6 illustrates the results of Table II, where the colored circles indicate the $J_{\rm em}(V_{\rm int})$ value. Then, we fit Eq. (9) to the $J_{\rm em}(V_{\rm int})$ shown in Fig. 6 to obtain the most probable

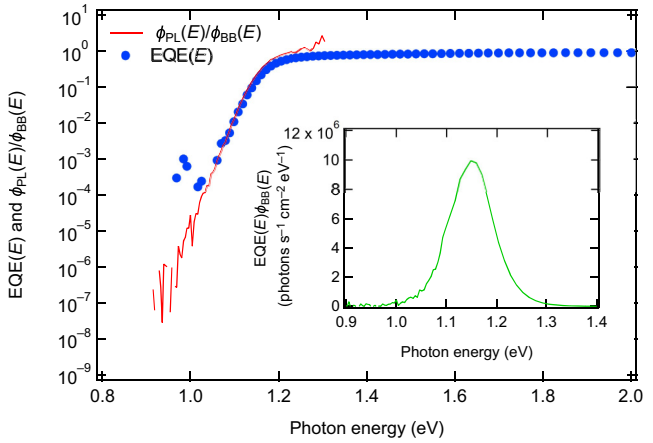


FIG. 4. Red curve is the result of dividing $\phi_{\rm PL}(E)$ by $\phi_{\rm BB}(E)$ at $T = 300$ K, where the red curve is multiplied by an appropriate coefficient. Blue circles are EQE($E$) shown in Fig. 2. Inset shows the EQE($E$)$\phi_{\rm BB}(E)$ where EQE($E$) is extended to the lower-energy side by the red curve.

values of $J_{0,\rm em}$ and $n$, yielding the following results:

$$J_{0,\rm em} = (2.9 \pm 1.5) \times 10^{-14}\ \text{mA/cm}^2, \tag{24}$$

$$n = 1.001 \pm 0.018, \tag{25}$$

where $1.5 \times 10^{-14}$ mA/cm$^2$ and 0.018 are the standard deviations of the uncertainty of the most probable values. Figure 6 shows the fitting results with a red curve, which indicates a good fit. For reference, the curve obtained by substituting Eq. (22) into Eq. (8) is also shown by the blue line in Fig. 6.

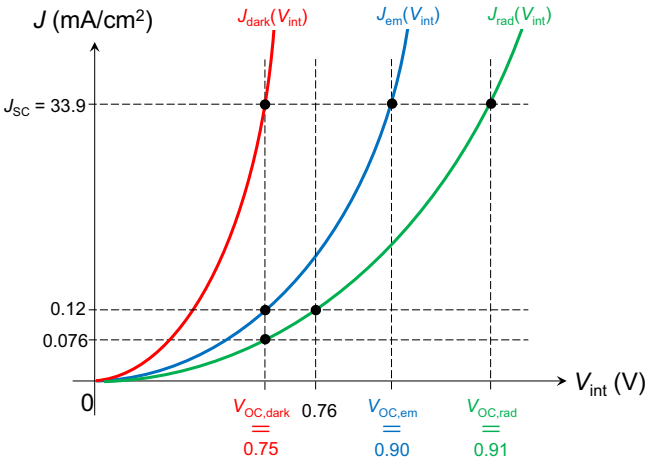


FIG. 5. Schematic representation of the results of this study. $\eta_{\rm ext} = 0.12/33.9 = 0.0035$. $\eta_{\rm ext}{}^* = 0.076/33.9 = 0.0023$. Hence, $\eta_{\rm ext}/\eta_{\rm ext}{}^* = 1.6$. $V_{\rm int} = 0.76$ V is the voltage satisfying $J_{\rm rad}(V_{\rm int}) = J_{\rm em}(V_{\rm OC,dark})$.

We estimate the value of $u_{\rm em}$ as follows. The value of $u_{\rm em}$ is influenced by two factors: (i) the measurement uncertainty $u_J$ of $J_{\rm em}(V_{\rm int})$ summarized in Table II, and (ii) the uncertainty $u_F$ of the most probable value of $J_{0,\rm em}$ obtained based on least-squares fitting. Therefore, we approximately estimate the value of $u_{\rm em}$ by

$$u_{\rm em} \approx \sqrt{u_J^2 + u_F^2}. \tag{26}$$

Equation (24) shows that $u_F$ is about 52%. Equation (14) suggests that the factors contributing to $u_J$ are the uncertainties of $T_0$, $A_c$, $\Omega_0$, and $n(V_{\rm int})$. Equation (15) indicates that the factors contributing to the uncertainty of $n(V_{\rm int})$ are the uncertainties of $L(V_{\rm int})$ and $S_{\rm eff}$. Let the relative standard uncertainties of $T_0$, $A_c$, $\Omega_0$, $L(V_{\rm int})$ and $S_{\rm eff}$ be $u_T$, $u_A$, $u_\Omega$. $u_L$, and $u_S$, respectively. $u_S$ corresponds to the calibration uncertainty of our photodetector, which measures the absolute value of the EL emission intensity. Because the operations used in Eqs (14) and (15) are the product and quotient, the value of $u_J$ is

$$u_J = \sqrt{u_T^2 + u_A^2 + u_\Omega^2 + u_L^2 + u_S^2}. \tag{27}$$

We estimate the value of $u_S$ using the following steps: First, we estimate the relative standard uncertainty of the relative value of $S(E)$, and set it to $u_1$. Then, we estimate the relative standard uncertainty of the standard light source used in step (2) (see Sec. II), and set it to $u_2$. Thus, $u_S$ is given by

$$u_S = \sqrt{u_1^2 + u_2^2}. \tag{28}$$

In this study, we estimate the values of $u_1$ and $u_2$ to be about 10%. Thus, the value of $u_S$ is estimated to be about 14%. The relative standard uncertainty $u_L$ of $L$ is estimated to be about 2%. It is difficult to accurately estimate the values of $u_T$, $u_A$, and $u_\Omega$; however, it is expected that the maximum values will not exceed 10%. Therefore, the maximum value of $u_J$ obtained from Eq. (27) is considered to be 25%. Thus, combined with the aforementioned result that the value of $u_F$ is about 52%, the value of $u_{\rm em}$ obtained from Eq. (26) is estimated to be about 57%. Thus, the value of $J_{0,\rm rad} = 1.8 \times 10^{-14}$ mA/cm$^2$ reported in Eq. (22) falls within the range of $J_{0,\rm em}(1 \pm u_{\rm em}) = (2.9 \pm 1.7) \times 10^{-14}$ mA/cm$^2$. Therefore, we can conclude that the optoelectronic reciprocity theorem given by Eq. (2) is quantitatively valid for the CIGS solar cells investigated in this study within the measurement uncertainty limits. Furthermore, Eq. (25) is experimental confirmation that the value of the diode ideality factor for the applied voltage dependence of the EL emission intensity is exactly unity when the emission mechanism is the band-edge emission due to

TABLE II. The values of $J_{\rm em}(V_{\rm int})$ for the cells SQ3720-3-1 to 8 (units are mA/cm$^2$). The density of injected current $J_{\rm dark}$ and the value of the applied voltage $V$ when we measure the EL emission intensity are also shown.

| $J_{\rm dark}$ (mA/cm$^2$) | $V$ (V) | $V_{\rm int}$ (V) | SQ3720-3-1 | SQ3720-3-2 | SQ3720-3-3 | SQ3720-3-4 | SQ3720-3-5 | SQ3720-3-6 | SQ3720-3-7 | SQ3720-3-8 |
|---|---|---|---|---|---|---|---|---|---|---|
| 9.579 | 0.714 | 0.707 | 0.026 | 0.022 | 0.021 | 0.021 | 0.017 | 0.019 | 0.019 | 0.016 |
| 19.157 | 0.744 | 0.731 | 0.063 | 0.057 | 0.057 | 0.055 | 0.052 | 0.057 | 0.053 | 0.047 |
| 28.736 | 0.765 | 0.745 | 0.105 | 0.097 | 0.099 | 0.098 | 0.095 | 0.100 | 0.092 | 0.084 |
| 38.314 | 0.781 | 0.755 | 0.151 | 0.142 | 0.149 | 0.144 | 0.143 | 0.149 | 0.137 | 0.125 |
| 47.893 | 0.795 | 0.762 | 0.200 | 0.190 | 0.199 | 0.194 | 0.195 | 0.200 | 0.184 | 0.170 |
| 57.471 | 0.808 | 0.768 | 0.249 | 0.240 | 0.254 | 0.246 | 0.250 | 0.256 | 0.233 | 0.216 |
| 67.050 | 0.819 | 0.773 | 0.301 | 0.294 | 0.307 | 0.301 | 0.306 | 0.315 | 0.285 | 0.263 |
| 76.628 | 0.830 | 0.777 | 0.355 | 0.348 | 0.364 | 0.356 | 0.365 | 0.376 | 0.338 | 0.314 |
| 86.207 | 0.875 | 0.782 | 0.409 | 0.404 | 0.420 | 0.415 | 0.428 | 0.438 | 0.395 | 0.366 |

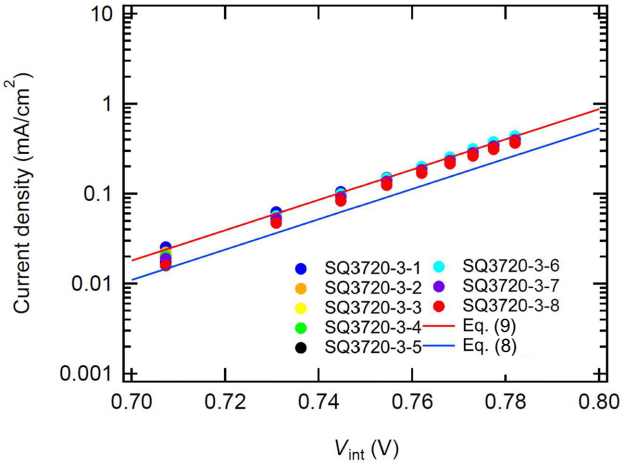


FIG. 6. Values of $J_{em}(V_{int})$ in Table II are shown by colored circles as a function of $V_{int}$. Red curve is the result of fitting Eq. (9) to the colored circles. Blue curve is obtained by substituting Eq. (22) into Eq. (8).

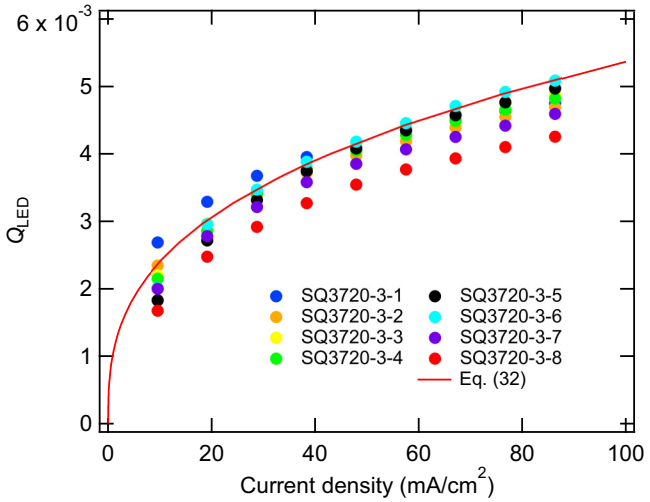


FIG. 7. Values of $Q_{LED}$ calculated using the data in Table II are shown by colored circles as a function of injected current density $J_{dark}$. The red curve is the result of substituting the results of Table I and Eq. (24) into $J_0$ and $J_{0,em}$ respectively in Eq. (32) and setting $n = 1.35$.

the direct recombination of electron-hole pairs. Substituting Eqs. (24) and (25) into Eq. (10), we can calculate the value of $V_{OC,em}$, which yields the following result:

$$V_{OC,em} = 0.90 \text{ V}. \tag{29}$$

This result is illustrated diagrammatically in Fig. 5, along with the blue curve showing $J_{em}(V_{int})$ given by Eq. (9).

The $J_{dark}$-dependence of $Q_{LED}$ calculated using the data in Table II yields the results shown by the colored circles in Fig. 7. Figure 7 shows that $Q_{LED}$ increases monotonically with increasing $J_{dark}$. The following explains the reason for the dependence on $J_{dark}$: First, the $J_{dark}$-$V_{int}$ characteristics $J_{dark}(V_{int})$ are generally given as

$$J_{dark}(V_{int}) = J_0 \exp\left(\frac{qV_{int}}{nk_BT}\right), \tag{30}$$

where $n$ is the diode ideality factor, which is $n = 1.35$ for the CIGS solar cells used in this study, as is shown in Table I. Then, $J_{em}(V_{int})$ is most generally given by Eq. (9), where $n = 1$ is confirmed by Eq. (25). Therefore, setting $n = 1$ in Eq. (9) and substituting the result and Eq. (30) into Eq. (18), the $V_{int}$ dependence of the $Q_{LED}$ is given by

$$Q_{LED}(V_{int}) = \left(\frac{J_{0,em}}{J_0}\right)\left\{\exp\left(\frac{qV_{int}}{k_BT}\right)\right\}^{(n-1/n)}. \tag{31}$$

Thus, substituting Eq. (30) into Eq. (31), $Q_{LED}$ is obtained as a function of $J_{dark}$ as

$$Q_{LED} = \left(\frac{J_{0,em}}{{J_0}^n}\right){J_{dark}}^{n-1}. \tag{32}$$

The red curve in Fig. 7 is obtained from the substitution of the result of Table I and Eq. (24) into $J_0$ and $J_{0,em}$, respectively, in Eq. (32) and setting $n = 1.35$. The agreement between the theoretical curve and the measurement results is excellent. Therefore, it is confirmed that the main reason for the $J$-dependence of the $Q_{LED}$ shown in Fig. 7 is because of the difference in the values of the diode ideality factor $n$ between $J_{dark}(V_{int})$ and $J_{em}(V_{int})$.

TABLE III. A comparison of the results obtained in this study with the device performance and $\eta_{ext}{}^*$ estimated for our best-performing CIGS solar cells (SQ3614-4) [38] and the CIGS solar cells reported in Ref. [39], whose conversion efficiency is currently the highest in the world.

| Devices | $E_g$ (eV) | $\eta$ (%) | $V_{OC}$ (V) | $J_{SC}$ (mA/cm$^2$) | FF | $V_{OC,em}$ (V) | $\eta_{ext}$ (%) | $V_{OC,rad}$ (V) | $\eta_{ext}{}^*$ (%) |
|---|---|---|---|---|---|---|---|---|---|
| This work | 1.15 | 19.5 | 0.75[a] | 33.9 | 0.77 | 0.90 | 0.35 | 0.91 | 0.22[b] |
| Ref. [39] | 1.08 | 23.35 | 0.734 | 39.6 | 0.804 | ··· | ··· | 0.85[c] | 1.13 |
| SQ3614-4 | 1.16 | 22.0 | 0.785 | 34.8 | 0.81 | ··· | ··· | 0.93[c] | 0.31 |

[a]The value of $V_{OC}$ in this work is the value of $V_{OC,dark}$ given by Eq. (33).
[b]The value of $\eta_{ext}{}^*$ in "This work" is $\eta_{ext}{}^* = \eta_{ext}/1.6$.
[c]The $V_{OC,rad}$ values for SQ3614-4 and Ref. [39] are estimated by $V_{OC,rad} = E_g/q - 0.23$.

If we define the voltage $V_{OC,dark}$ as the voltage that satisfies $J_{dark}(V_{OC,dark}) = J_{SC}$, then it is given by the results of Eq. (30) and Table I as

$$V_{OC,dark} = 0.75\ V \tag{33}$$

This result is illustrated diagrammatically in Fig. 5, along with the red curve showing $J_{dark}(V_{int})$ given by Eq. (30). This value is close to the $V_{OC} = 0.74$ V in Table I, but slightly different. The reason for the difference is that the shifting approximation [37] does not hold. That is, the light $J$-$V$ curve shifted by $J_{SC}$ is slightly different from the $J_{dark}$-$V_{int}$ curve. Finally, the value of $\eta_{ext}$ for this device obtained from Fig. 7 is $\eta_{ext} = 0.0035$. Substituting this value and $V_{OC,em} = 0.90$ V given by Eq. (29) into Eq. (1) to calculate the value of $V_{OC}$, we obtain the value in Eq. (33). Furthermore, by substituting the above $\eta_{ext}$ values into Eq. (5) along with $V_{OC,rad} = 0.91$ V given by Eq. (23), we obtain $V_{OC} = 0.76$ V. This is the voltage that satisfies $J_{rad}(V) = J_{em}(V_{OC,dark})$ as illustrated diagrammatically in Fig. 5.

If we define $\eta_{ext}^{*}$ as the result obtained from solving Eq. (5) for $\eta_{ext}$, we have

$$\eta_{ext}^{*} = \exp\left\{\left(\frac{q}{k_B T}\right)(V_{OC} - V_{OC,rad})\right\}. \tag{34}$$

Substituting $V_{OC,dark}$ in Eq. (33) and $V_{OC,rad}$ in Eq. (23) into $V_{OC}$ and $V_{OC,rad}$ in Eq. (34), respectively, yields $\eta_{ext}^{*} = 0.0023$, which agrees with the value of $\eta_{ext} = 0.0035$ within the limits of our measurement uncertainty. These results are shown diagrammatically in Fig. 5, with the value of $J_{em}(V_{OC,dark}) = 0.12$ mA/cm$^2$ and $J_{rad}(V_{OC,dark}) = 0.076$ mA/cm$^2$. The voltage $V_{int} = 0.76$ V satisfying $J_{rad}(V_{int}) = J_{em}(V_{OC,dark})$ is also shown in Fig. 5. Table III summarizes these results with the device performance and the value of $\eta_{ext}^{*}$ estimated for both our best-performing CIGS solar cell (SQ3614-4) [38] and the world's highest-efficiency CIGS solar cell reported by Nakamura *et al.* [39]. Here, the values of $V_{OC,rad}$ for SQ3614-4 and the device reported by Nakamura *et al.* [39] are estimated by $V_{OC,rad} = E_g/q - 0.23$. Also, the value of $V_{OC}$ in "this work" in Table III is the value of $V_{OC,dark}$ given by Eq. (33). Table III shows that the cells with higher conversion efficiency also have higher $\eta_{ext}^{*}$ values. Figure 8 shows chronological improvements in conversion efficiency for CIGS solar cells reported in previous studies [39–42] and $\eta_{ext}$ values analyzed for CIGS solar cells. The $\eta_{ext}$ values show a good measure for efficiency potential for CIGS solar cells. High- efficiency CIGS solar cells with an efficiency of >26% can be realized by increasing the $\eta_{ext}$ from 1% to 10%.

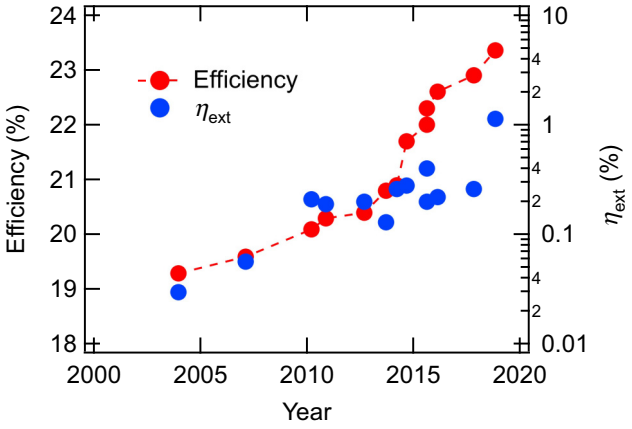


FIG. 8. Chronological improvements in conversion efficiency for CIGS solar cells reported in previous studies [39–42] and $\eta_{ext}$ values analyzed for the CIGS solar cells. The $\eta_{ext}$ values show a good measure for efficiency potential for CIGS solar cells.

## IV. CONCLUSION

We experimentally confirm whether the optoelectronic reciprocity theorem holds for the high-efficiency CIGS solar cells we fabricated. The results indicate that the CIGS solar cells qualitatively and quantitatively satisfy the optoelectronic reciprocity theorem within the limits of our measurement uncertainty. The value of $V_{OC,rad}$ calculated from the EQE spectrum is $V_{OC,rad} = 0.91$ V, thus $\Delta V_{OC,rad} \equiv E_g/q - V_{OC,rad} = 0.24$ V, where $E_g \approx 1.15$ eV is the band-gap energy of the CIGS solar cell studied in this paper. This value is very close to the value assumed in our previous study [20–23] (0.23 V) and that reported by Yao *et al.* [14] (0.231 V). We also confirm that the value of the diode ideality factor for the applied voltage dependence of the EL emission intensity is exactly unity when the emission mechanism is the band-edge emission due to the direct recombination of electron-hole pairs. The importance of $\eta_{ext}$ for improving solar cell efficiency is explained in this study.

## ACKNOWLEDGMENTS

The authors thank Kan-Hua Lee for fruitful discussions and careful reading of the manuscript. The authors also thank M. Iioka, H. Takahashi, and H. Higuchi for their technical assistance. This work was supported by the New Energy and Industrial Technology Development Organization (NEDO) under the Ministry of Economy, Trade and Industry (METI), Japan.

[1] N. M. Heagel, *et al.*, Terawatt-scale photovoltaics: Transform global energy, Science **364**, 836 (2019).

[2] W. Shockley and H. J. Queisser, Detailed balance limit of efficiency of p-n junction solar cells, J. Appl. Phys. **32**, 510 (1961).

[3] U. Rau, Reciprocity relation between photovoltaic quantum efficiency and electroluminescent emission of solar cells, Phys. Rev. B **76**, 085303 (2007).

[4] T. Kirchartz and U. Rau, Electroluminescence analysis of high efficiency Cu(In, Ga)$Se_2$ solar cells, J. Appl. Phys. **102**, 104510 (2007).

[5] T. Kirchartz, U. Rau, M. Kurth, J. Mattheis, and J. H. Werner, Comparative study of electroluminescence from Cu(In, Ga)$Se_2$ and Si solar cells, Thin Solid Films **515**, 6238 (2007).

[6] T. Kirchartz and Uwe Rau, Detailed balance and reciprocity in solar cells, Phys. Status Solidi A **205**, 2737 (2008).

[7] T. Kirchartz, A. Helbig, W. Reetz, M. Reuter, J. H. Werner, and U. Rau, Reciprocity between electroluminescence and quantum efficiency used for the characterization of silicon solar cells, Prog. Photovoltaics **17**, 394 (2009).

[8] M. A. Green, Radiative efficiency of state-of-the-art photovoltaic cells, Prog. Photovoltaics **20**, 472 (2012).

[9] A. Delamarre, L. Lombez, and J.-F. Guillemoles, Characterization of solar cells using electroluminescence and photoluminescence hyperspectral images, J. Photonics Energy **2**, 027004 (2012).

[10] J. Wong and M. A. Green, From junction to terminal: Extended reciprocity relations in solar cell operation, Phys. Rev. B **85**, 235205 (2012).

[11] J. F. Geisz, M. A. Steiner, I. Garcia, S. R. Kurtz, and D. J. Friedman, Enhanced external radiative efficiency for 20.8% efficient single-junction GaInP solar cells, Appl. Phys. Lett. **103**, 041118 (2013).

[12] X. Wang and M. S. Lundstrom, On the use of Rau's reciprocity to deduce external radiative efficiency in solar cells, IEEE J. Photovoltaics **3**, 1348 (2013).

[13] T. C. M. Müller, B. E. Pieters, T. Kirchartz, R. Carius, and U. Rau, Effect of localized states on the reciprocity between quantum efficiency and electroluminescence in Cu(In, Ga)$Se_2$ and Si thin-film solar cells, Sol. Energy Mater. Sol. Cells **129**, 95 (2014).

[14] J. Z. Yao, T. Kirchartz, M. S. Vezie, M. A. Faist, W. Gong, Z. C. He, H. B. Wu, J. Troughton, T. Watson, D. Bryant, and J. Nelson, Quantifying Losses in Open-Circuit Voltage in Solution-Processable Solar Cells, Phys. Rev. Appl. **4**, 014020 (2015).

[15] S. Chen, L. Zhu, M. Yoshita, T. Mochizuki, C. Kim, H. Akiyama, M. Imaizumi, and Y. Kanemitsu, Thorough subcells diagnosis in a multi-junction solar cell via absolute electroluminescence-efficiency measurements, Sci. Rep. **5**, 7836 (2015).

[16] T. Mochizuki, C. Kim, M. Yoshita, J. Mitchell, Z. Lin, S. Chen, H. Takato, Y. Kanemitsu, and H. Akiyama, Solar-cell radiance standard for absolute electroluminescence measurements and open-circuit voltage mapping of silicon solar modules, J. Appl. Phys. **119**, 034501 (2016).

[17] D. Abou-Ras, T. Kirchartz, and U. Rau, *Advanced Characterization Techniques for Thin Film Solar Cell* (Wiley-VCH Verlag GmbH & Co, Weinheim, Germany, 2016), pp. 71.

[18] U. Aeberhard and U. Rau, Microscopic Perspective on Photovoltaic Reciprocity in Ultrathin Solar Cells, Phys. Rev. Lett. **118**, 247702 (2017).

[19] U. Rau, B. Blank, T. C. M. Müller, and T. Kirchartz, Efficiency Potential of Photovoltaic Materials and Devices Unveiled by Detailed-Balance Analysis, Phys. Rev. Appl. **7**, 044016 (2017).

[20] M. Yamaguchi, H. Yamada, Y. Katsumata, K. Lee, K. Araki, and N. Kojima, Efficiency potential and recent activities of high-efficiency solar cells, J. Mater. Res. **32**, 3445 (2017).

[21] M. Yamaguchi, L. Zhu, H. Akiyama, Y. Kanemitsu, H. Tampo, H. Shibata, K. Lee, K. Araki, and N. Kojima, Analysis of future generation solar cells and materials, Jpn. J. Appl. Phys. **57**, 04FS03 (2018).

[22] M. Yamaguchi, K. Lee, K. Araki, N. Kojima, H. Yamada, and Y. Katsumata, Analysis for efficiency potential of high-efficiency and next-generation solar cells, Prog. Photovoltaics **26**, 543 (2018).

[23] M. Yamaguchi, H. Tampo, H. Shibata, K. Lee, K. Araki, N. Kojima, and Y. Ohshita, Analysis for non-radiative recombination and resistance loss in chalcopyrite and kesterite solar cells, Jpn. J. Appl. Phys. **60**, SBBF05 (2021).

[24] M. A. Green and A. W. Y. Ho-Baillie, Pushing to the limit: Radiative efficiencies of recent mainstream and emerging solar cells, ACS Energy Lett. **4**, 1639 (2019).

[25] K. Toprasertpong, A. Delamarre, Y. Nakano, J.-F. Guillemoles, and M. Sugiyama, Generalized Reciprocity Relations in Solar Cells with Voltage-Dependent Carrier Collection: Application to *p-i-n* Junction Devices, Phys. Rev. Appl. **11**, 024029 (2019).

[26] J. Bisquert, *The Physics of Solar Energy Conversion* (CRS Press, Boca Raton, FL, 2020), pp. 375.

[27] M. Ochoa, S. Yang, S. Nishiwaki, A. N. Tiwari, and R. Carron, Challenges and opportunities for an efficiency boost of next generation Cu(In, Ga)$Se_2$ solar cells: Prospects for a paradigm shift, Energy Environ. Sci. **13**, 2047 (2020).

[28] W. van Roosbroeck and W. Shockley, Photon-Radiative Recombination of Electrons and Holes in Germanium, Phys. Rev. **94**, 1558 (1954).

[29] G. Lasher and F. Stern, Spontaneous and Stimulated Recombination Radiation in Semiconductors, Phys. Rev. **133**, A553 (1964).

[30] P. Würfel, The chemical potential of radiation, J. Phys. C, Solid State Phys. **15**, 3967 (1982).

[31] M. A. Green, J. Zhao, A. Wang, P. J. Reece, and M. Gal, Efficient silicon light-emitting diodes, Nature **412**, 805 (2001).

[32] U. Rau and J. H. Werner, Radiative efficiency limits of solar cells with lateral band-gap fluctuations, Appl. Phys. Lett. **84**, 3735 (2004).

[33] J. H. Werner, J. Mattheis, and U. Rau, Efficiency limitations of polycrystalline thin film solar cells: case of Cu(In,Ga)$Se_2$, Thin Solid Films **480–481**, 399 (2005).

[34] J. Mattheis, T. Schlenker, M. Bogicevic, U. Rau, and J. H. Werner, Band gap fluctuations in Cu(In, Ga)$Se_2$ thin films, Mater. Res. Soc. Symp. Proc. **865**, F16.4.1 (2005).

[35] A. M. Gabor, J. R. Tuttle, M. H. Bode, A. Franz, A. L. Tennant, M. A. Contreras, R. Noufi, D. G. Jensen, and A. M. Hermann, Band-gap engineering in Cu(In, Ga)$Se_2$

thin films grown from $(In, Ga)_2Se_3$ precursors, Sol. Energy Mater. Sol. Cells **41–42**, 247 (1996).

[36] ATTO Corporation, 3-3-2 Motoasakusa, Taito-ku, Tokyo 111-0041, Japan.

[37] E. A. Lindholm, J. G. Fossum, and E. L. Burgess, Application of the superposition principle to solar-cell analysis, IEEE Trans. Electron Devices **ED-26**, 165 (1979).

[38] . J. Nishinaga (unpublished).

[39] M. Nakamura, K. Yamaguchi, Y. Kimoto, Y. Yasaki, T. Kato, and H. Sugimoto, Cd-free $Cu(In, Ga)(Se, S)_2$ thin-film solar cell with record efficiency of 23.35%, IEEE J. Photovoltaics **9**, 1863 (2019).

[40] K. Ramanathan, J. Keane, and R. Noufi, in *presented at the 31st IEEE Photovoltaic Specialists Conference, Florida, Jan. 3–7* (2005). https://www.nrel.gov/docs/fy05osti/37404.pdf.

[41] P. Jackson, D. Hariskos, R. Wuerz, O. Kiowski, A. Bauer, T. M. Friedlmei, and M. Powalla, Properties of $Cu(In, Ga)Se_2$ solar cells with new record efficiencies up to 21.7%, Phys. Status Solidi RRL **9**, 28 (2015).

[42] R. Kamada, T. Yagioka, S. Adachi, A. Handa, K. F. Tai, T. Kato, and H. Sugimoto, in *Proc. 43rd IEEE Photovoltaic Specialists Conference* (IEEE, New York, 2016), pp. 1287.